**Atmospheric
Measurement
Techniques
Discussions**

A Fourier transform infrared trace gas analyser for atmospheric applications

D. W. T. Griffith[1], N. M. Deutscher[1,*], C. G. R. Caldow[1], G. Kettlewell[1],
M. Riggenbach[1], and S. Hammer[2]

[1]University of Wollongong, Wollongong, NSW 2522, Australia
[2]University of Heidelberg, Institute of Environmental Physics, Heidelberg, Germany
[*]now at: University of Bremen, Institute of Environmental Physics, Bremen, Germany

Correspondence to: D. W. T. Griffith (griffith@uow.edu.au)

AMTD

5, 3717–3769, 2012

A Fourier transform infrared trace gas analyser

D. W. T. Griffith et al.

Title Page

Abstract	Introduction
Conclusions	References
Tables	Figures

|◄ | ►|
◄ | ►
Back | Close

Full Screen / Esc

Printer-friendly Version

Interactive Discussion

Abstract

Concern in recent decades about human impacts on Earth's climate has led to the need for improved and expanded measurement capabilities for greenhouse gases in the atmosphere. In this paper we describe in detail an in situ trace gas analyser based on Fourier Transform Infrared (FTIR) spectroscopy that is capable of simultaneous and continuous measurements of carbon dioxide (CO_2), methane (CH_4), carbon monoxide (CO), nitrous oxide (N_2O) and ^{13}C in CO_2 in air with high precision and accuracy. Stable water isotopes can also be measured in undried airstreams. The analyser is automated and allows unattended operation with minimal operator intervention. Precision and accuracy meet and exceed the compatibility targets set by the World Meteorological Organisation – Global Atmosphere Watch Programme for baseline measurements in the unpolluted troposphere for all species except ^{13}C in CO_2.

The analyser is mobile and well suited to fixed sites, tower measurements, mobile platforms and campaign-based measurements. The isotopic specificity of the optically-based technique and analysis allows application of the analyser in isotopic tracer experiments, for example ^{13}C in CO_2 and ^{15}N in N_2O. We review a number of applications illustrating use of the analyser in clean air monitoring, micrometeorological flux and tower measurements, mobile measurements on a train, and soil flux chamber measurements.

1 Introduction

Growing concern in recent decades about human impacts on Earth's climate has led to the need for improved understanding of greenhouse gases in the atmosphere and the global carbon cycle. The Fourth Assessment Report of the Intergovernmental Panel on Climate Change (IPCC, 2007) provides the most recent and extensive overview of the physical basis of human-induced climate change. Carbon dioxide (CO_2) and methane (CH_4) are the most important anthropogenic long lived greenhouse gases

(GHGs), accounting for 64 % and 18 % of human-induced radiative forcing since the preindustrial era (Hoffman et al., 2006, for update see http://www.esrl.noaa.gov/gmd/aggi/). Nitrous oxide (N_2O) is the third most important greenhouse gas with a 6 % contribution that is increasing as the now-restricted chlorofluorocarbons decay in the

5 atmosphere in coming decades (Ravishankara et al., 2009). The most important source of anthropogenic CO_2 increases is fossil fuel combustion for energy; for CH_4 increased wetlands and agricultural livestock emissions predominate, and for N_2O the increased use of nitrogeneous fertilisers in agriculture is the major contributor. These emissions are partially taken up and recycled by the oceans, land and the biosphere, and while

10 CH_4 and N_2O are ultimately chemically destroyed in the atmosphere, approximately half of fossil fuel CO_2 accumulates in the atmosphere (IPCC, 2007).

Measurements of greenhouse gases in the atmosphere provide the fundamental data on which our understanding is based. In situ measurements at the local or ecosystem level lead to "bottom-up" detailed understanding of the individual processes and

15 magnitudes of GHG exchanges, but are necessarily sparse and require significant up-scaling and extrapolation to be used in global-scale models of GHG source-sink distributions and inventories. In the alternative "top-down" approach, time series of in situ and remote sensing measurements are combined with inverse models and atmospheric transport to infer source-sink distributions at global scales, but here the problem

20 is mathematically ill-posed, and uncertainties are dominated by the sparseness of the available measurements. Both top down and bottom up approaches benefit from new techniques which can increase the density and accuracy of available measurements. In particular, the extension of measurements from occasional, often flask-based sampling programmes to continuous measurements near the ground, on tall towers, and

25 from satellites is highly desirable. Continuous measurements of trace gases resolve their variability on diurnal and synoptic timescales, which are becoming increasingly accessible to high resolution models. However the accuracy requirements are stringent – the World Meteorological Organisation's Global Atmosphere Watch (GAW) specifies the required inter-station compatibility and lack of bias required for measurements to

A Fourier transform infrared trace gas analyser

D. W. T. Griffith et al.

Title Page

Abstract | Introduction

Conclusions | References

Tables | Figures

|◄ | ►|

◄ | ►

Back | Close

Full Screen / Esc

Printer-friendly Version

Interactive Discussion

improve understanding of global greenhouse gas cycling. These requirements and approximate global mean atmospheric mole fractions (2010) are listed in Table 1 (GAW, 2011).

Regular atmospheric GHG measurements effectively began in the International Geophysical Year of 1957 with the establishment of CO_2 measurements by non dispersive infrared spectroscopy (NDIR) at Mauna Loa in Hawaii by C. D. Keeling (Keeling et al., 1995), and are now continuous at several global sites (e.g. Francey et al., 2010; Steele et al., 2011, see also http://www.esrl.noaa.gov/gmd/). For other species, high accuracy greenhouse gas measurements have been dominated by gas chromatography (GC) techniques using various detectors. GC is not a continuous technique and requires frequent calibration, but can be automated and is commonly used to provide pseudo-continuous regular measurements for most species in many stations and networks (see for example van der Laan et al., 2009; Vermeulen et al., 2011; Popa et al., 2010; Prinn et al., 2000; Langenfelds et al., 2011).

Optical techniques based on the absorption or emission of radiation are well suited to continuous measurements and have a robust physical basis for calibration. Recent advances in laser-based techniques have achieved the required precision in many cases and several instruments have become commercially available. Lasers are inherently single-wavelength devices that can be scanned over single absorption lines in a narrow wavelength interval. They are typically restricted to only one or two species, but high brightness of the laser source leads to low noise and high precision measurements. Earlier instruments used liquid nitrogen-cooled lead-salt mid-IR lasers ($\lambda > 2.0\,\mu m$), but these have been largely supplanted by cheaper, mass produced and readily available near-IR ($\lambda \sim 0.7$–$2.0\,\mu m$) lasers operating near room temperature. While the near-IR lasers are relatively cheap and freely available, absorption bands in the near-IR are generally overtone and combination bands which are weak absorbers compared to the fundamental vibration bands in the mid-IR. The weak absorption cancels some of the advantage of high brightness and low noise, and long absorption paths are required to obtain the desired precision. Most recently, quantum cascade lasers operating near

A Fourier transform infrared trace gas analyser

D. W. T. Griffith et al.

Title Page

Abstract | Introduction

Conclusions | References

Tables | Figures

|◄ | ►|

◄ | ►

Back | Close

Full Screen / Esc

Printer-friendly Version

Interactive Discussion

room temperature at mid-IR wavelengths have been developed, and these are becoming commercially available (e.g. Tuzson et al., 2011).

Fourier Transform InfraRed (FTIR) spectroscopy offers an alternative infrared optical technique to laser spectroscopy. FTIR uses broadband infrared radiation from a blackbody light source that covers the entire infrared spectrum simultaneously. In FTIR spectroscopy radiation from the source is modulated by a Michelson interferometer and all optical frequencies are recorded simultaneously in the measured interferogram (Davis et al., 2001; Griffiths and de Haseth, 2007). A mathematical Fourier transform retrieves the spectrum (intensity vs frequency) from the interferogram. Compared to laser sources the blackbody source is less bright, but this disadvantage is largely offset by the multiplex advantage of measuring the whole spectrum simultaneously, and operation in the mid-IR region where absorption bands are strong compared to the near-IR. The result is precision similar to or better than NIR-laser based instruments, but with the ability to determine several species, including isotopologues, simultaneously from the same measured spectrum.

Figure 1 shows the mid infrared spectrum of clean air in a 24 m path absorption cell as recorded with the analyser described in this paper. The target gases, carbon dioxide (CO_2), methane (CH_4), nitrous oxide (N_2O), carbon monoxide (CO), and water vapour (H_2O) have absorption bands in this region. Infrared absorption frequencies depend on the atomic masses, and in the case of $^{13}CO_2$ the ν_3 stretching vibration is shifted 66 cm^{-1} from the parent $^{12}CO_2$ band, which allows independent determination of ^{13}C fractionation in CO_2 with a low resolution FTIR spectrometer. H^{2}HO (HDO) absorption is also well separated from that of H_2O and allows measurements of H/D fractionation (Parkes et al., 2012). Quantitative analysis of broad regions of the spectrum (typically 100–200 cm^{-1} wide) including whole absorption bands of the molecules of interest provides the concentrations of the target species. The spectral information from many ro-vibronic lines is included in each analysis, enhancing the information content of the measurement compared to narrow-band, single line laser methods, thus leading to high measurement precision and stability.

A Fourier transform infrared trace gas analyser

D. W. T. Griffith et al.

Title Page

Abstract	Introduction
Conclusions	References
Tables	Figures

|◄ | ►|
| ◄ | ► |

Back | Close

Full Screen / Esc

Printer-friendly Version

Interactive Discussion

D. W. T. Griffith et al.

In this paper we describe the construction, performance and selected applications of a high precision trace gas analyser based on low resolution Fourier Transform Infrared (FTIR) spectrometry. The FTIR spectrometer is coupled to a multi-pass (White) cell and a gas sampling manifold and is principally intended for in situ sampling and analysis of ambient air. The analyser is fully automated and provides real-time concentration or mole fraction measurements of target gases including CO_2, CO, CH_4, N_2O, H_2O and the isotopologues $^{13}CO_2$, HDO and $H_2^{18}O$. The analyser is an extension of earlier work (Esler et al., 2000a,b; Griffith and Galle, 2000) and incorporates significant improvements in usability and performance. Parkes et al. describe optimisation of the analyser for stable water isotope measurements (Parkes et al., 2012).

2 Description of the analyser

The FTIR spectrometer is a Bruker IRcube, a modular unit built around a frictionless flex-pivot interferometer with $1\,cm^{-1}$ resolution ($0.5\,cm^{-1}$ optional) and $25\,mm$ beam diameter, globar source and CaF_2 beamsplitter. The modulated exit beam is coupled to a multipass White cell by transfer optics consisting of two flat mirrors. The White cell is a permanently aligned glass cell, f-matched to the FTIR beam with a total folded path of $24\,m$ and volume $3.5\,l$. The beam exiting the White cell is directed back into the IRcube and focussed onto a $1\,mm$ diameter thermoelectrically-cooled MCT detector with peak detectivity at $2000\,cm^{-1}$. The root mean square (RMS) signal-to-noise ratio in the spectra for a 1-min measurement ($\sim$80 coadded spectra) through the cell at $1\,cm^{-1}$ resolution is typically $40\,000$–$60\,000 : 1$ (measured as 1/noise where noise is the rms noise from 2500–$2600\,cm^{-1}$ on the ratio of two consecutively collected spectra). The signal-to-noise ratio (SNR) increases as the square root of averaging time for coadded spectra up to at least 20 min.

The White cell is fitted with a 0–$1333\,hPa$ piezo-manometer to measure cell pressure and a type-J or type-T thermocouple in the cell for cell temperature measurement. Ambient water vapour, CO_2, CO, CH_4 and N_2O are removed from the internal volume

of the IRcube and transfer optics with a slow purge of dry N_2 (0.1–0.2 l min^{-1}) backed by a molecular sieve and Ascarite® trap in the volume. The FTIR and sample cell are thermostatted, typically at 30 °C.

The evacuation and filling of the cell with sample or calibration gas is controlled by a manifold of solenoid valves, shown schematically in Fig. 2. A 4-stage oil-free diaphragm pump with ultimate vacuum of approximately 1 hPa is used to evacuate and draw sample gas through the cell. Sample or calibration gas streams are introduced through one of four equivalent inlets (V1–V4), optionally dried by passing through a Nafion® drier and $Mg(ClO_4)_2$ trap (selected by V9). The gas stream passes through a 7 µm sintered stainless steel particle filter into the sample cell (V6). Flow is controlled by a mass flow controller which can optionally function as a cell pressure controller through a feedback loop to the cell pressure transducer. In earlier versions of the analyser, a needle valve and mass flow meter were used instead of the mass flow controller. Flow rate is typically 0.5–1.5 l min^{-1} and cell pressure is near ambient pressure. The dried sample gas stream leaving the cell provides the required back-flush to the Nafion dryer at reduced pressure. The Nafion drier alone typically achieves water vapour mole fractions of 200–300 µmol mol^{-1} (dew point < −40 °C) in the sampled airstream, and the $Mg(ClO_4)_2$ typically reduces this to <10 µmol mol^{-1}. Sample or calibration gas may also be analysed statically by evacuating and filling the cell without flow during the measurement. In this case a flow of dried air can be maintained through the Nafion drier via a cell-bypass valve (V5) to avoid step changes in water vapour levels which may occur if the Nafion drier is not continuously flushed. The cell can be evacuated directly through V8.

The solenoid manifold valves are switched by a digital output (DO) relay module connected to the controlling computer via a RS232-RS485 serial interface. An 8-channel, 16-bit analogue-digital converter (ADC) module is connected via the same RS485 daisy-chain to log pressure, cell and room temperatures, flow and other analogue signals. The mass flow controller is controlled by an analogue output (AO) module. Additional DO, AO or ADC modules can be added as required to the RS485 daisy chain

A Fourier transform infrared trace gas analyser

D. W. T. Griffith et al.

Discussion Paper | Discussion Paper | Discussion Paper | Discussion Paper

for special applications. Operation of the spectrometer, sample manifold, data logging, spectrum analysis (described below) and real time display of gas concentrations is controlled by a single program ("Oscar") written in Microsoft Visual Basic. The spectrometer communication is via Bruker's OPUS DDE interface over a private Ethernet network. The DO, AO and ADC modules are connected via the PC's serial RS232 port. Oscar provides for the configuration and fully automated execution of user-defined sequences of valve-switching for flow control, spectrum collection, spectrum quantitative analysis, logging and display. Different sequences may be executed in turn and looped to provide continuous automated operation, including periodic calibration tank measurements, without manual intervention. The instrument can be run remotely via an ethernet connection to the PC.

2.1 Quantitative spectrum analysis

Spectra are analysed to determine the amounts of selected trace gases in the cell by non-linear least squares fitting of broad regions (100–200 cm^{-1}) of the spectrum selected for each target gas. The analysis is carried out automatically after spectrum collection, and the results logged and displayed on the controlling computer. Spectroscopic analysis fundamentally determines the total absorber amount (concentration × pathlength, $C \times L$) of the target trace gas, from which the mole fraction χ of the trace gas in air is calculated from the molar concentration of air, $n/V = P/RT$

$$\chi = \frac{C}{P/RT} \tag{1}$$

where P is the measured sample pressure, T the sample cell temperature, and R the universal gas constant. From Eq. (1), χ is the mole fraction in whole air – χ can be converted to dry air mole fraction using the measured mole fraction of water vapour in the sampled air in the cell determined simultaneously from the FTIR spectrum as in Eq. (2)

$$\chi_{dry} = \frac{\chi}{(1 - \chi_{H_2O})}.$$
(2)

For dried air χ_{H_2O} is generally small ($< 10\,\mu mol\,mol^{-1}$) and the correction to dry air mole fraction is small. The quantitative spectrum analysis takes a computational approach in which the spectral region to be analysed is iteratively fitted with a calculated spectrum. The spectrum model, MALT (Multiple Atmospheric Layer Transmission), and non-linear least squares retrieval of concentrations from spectra, are described in detail elsewhere (Griffith, 1996, 2012) and only summarised here. For most trace gases of interest, the positions, strengths, widths and temperature dependences of relevant absorption lines are available in the HITRAN database (Rothman et al., 2005). From the HITRAN line parameters, the MALT spectral model calculates the absorption coefficients of the gas sample in the cell at the measured temperature and pressure. For samples containing gases that are not included in HITRAN, the absorption coefficients can be calculated from quantitative library reference spectra if available – for example, the Northwest Infrared Vapour Phase Reference Library provides such data for over 400 compounds (https://secure2.pnl.gov/nsd/nsd.nsf/Welcome, see also Sharpe et al., 2004; Johnson et al., 2010). The monochromatic (i.e. true, infinite resolution) transmittance spectrum is calculated from the absorption coefficients and initial estimates of trace gas concentrations, then convolved with the FTIR instrument lineshape (ILS) function, which includes the effects of resolution (maximum optical path difference of the interferogram), apodisation, and finite field of view (beam divergence in the interferometer). In addition, effects of imperfect alignment or optics can be included, for example wavenumber scale shift, loss of modulation efficiency at high optical path difference, and residual phase error, which may lead to shifted, broadened and asymmetric lineshapes, respectively. The resulting calculated spectrum simulates the measured spectrum, and is iteratively re-calculated using a Levenberg-Marquardt algorithm (Press et al., 1992) to update estimates of absorber amounts and ILS parameters until the best fit (minimum sum of squared residuals between measured and calculated spectra) is achieved.

The transmittance model is not linear in the fitted parameters (absorber amounts and ILS), necessitating the iterative non-linear least squares fitting. This method is fundamentally different from methods commonly used in chemometric approaches to quantitative spectrum analysis, and in particular the Classic Least Squares (CLS) or Partial Least Squares (PLS) used in earlier work (Griffith, 1996). These chemometric approaches are applied to absorbance spectra and fit the spectrum as a linear combination of single component absorbance spectra (CLS) or factors (PLS). They inherently assume that Beer's Law (i.e. that absorbance is approximately proportional to concentrations of absorbers) is obeyed or nearly obeyed, but cannot fit spectral variations due to ILS effects, and are restricted to regions of weak absorption to avoid non-linearities and breakdown of Beer's Law (Anderson and Griffiths, 1975; Haaland, 1987). In non-linear least squares the spectrum can be fitted in any region, not just one of weak absorption, because there is no assumption of linearity between transmittance and trace gas concentrations. All spectral points have the same measurement noise error independent of the transmittance, and therefore have equal weight in calculating and minimising the residual sum of squares.

The iterative fit normally takes 5–10 iterations and a few seconds of computation time on a typical personal computer. Figure 3 illustrates spectral fits to typical regions: (a) 2150–2310 cm^{-1} for CO_2 isotopologues, CO and N_2O, (b) 2097–2242 cm^{-1} optimised for N_2O and CO (c) 3001–3150 cm^{-1} for CH_4, and (d) 3520–3775 cm^{-1} for CO_2 (all isotopologues) and H_2O. In undried air, H_2O, HDO and $H_2^{18}O$ can be independently determined to provide fractionations of the hydrogen and oxygen isotopes in water vapour (Parkes et al., 2012, not shown). In the region near 2300 cm^{-1} the ^{13}C and ^{12}C isotopologues of CO_2 are well resolved (the $^{13}CO_2$ asymmetric stretching band is shifted 66 cm^{-1} from the corresponding $^{12}CO_2$ band) and can be fitted independently, allowing a direct measurement of ^{13}C fractionation in atmospheric CO_2. In general, overlap of absorption bands of different gases is accounted for by the MALT spectral model and isolated spectral features are not required for analysis. However cross-sensitivities may be significant with overlap of a weak band by a much stronger

band, such as is the case for N_2O and $^{13}CO_2$ shown Fig. 3a – in this case an additional window from 2097–2242 cm^{-1} can be used to minimise this cross-sensitivity, shown in Fig. 3b.

All spectra are stored after measurement and archived. An advantage of the method is that spectra can be re-analysed at any later time, for example with a different choice of spectral regions or with improved line parameters as they may become available.

The fitting procedure provides trace gas amounts and ILS parameters without any reference to calibration spectra of reference gases. For an ideal measured spectrum from a perfectly aligned spectrometer, the fitted spectrum residual should show only random detector noise and absolute accuracy would depend only on the HITRAN line parameters, pressure, temperature and pathlength measurements. In reality, the raw FTIR determination of trace gas concentrations is highly precise, but typically accurate only to within a few percent due to systematic errors in the spectrometer, MALT model, HITRAN data and measured pressure and temperature (Smith et al., 2011). Higher accuracy, equivalent to the precision of repeated measurements, is achieved by analysis of calibration standards that have known concentrations traceable to accepted reference scales (GAW, 2011). Calibration equations can be derived by analysis of one or more such standards. Details of precision and accuracy are given in the following section.

The analyser and spectral analysis procedure has been developed and improved over several years since the first versions described by Esler et al. (2000a, b). Since 2011 the analyser described above, with refinements, is available commercially as the Spectronus analyser from Ecotech Pty Ltd., Knoxfield, Australia.

A Fourier transform infrared trace gas analyser

D. W. T. Griffith et al.

Title Page

Abstract | Introduction

Conclusions | References

Tables | Figures

◄ | ►►

◄ | ►

Back | Close

Full Screen / Esc

Printer-friendly Version

Interactive Discussion

3 Precision, accuracy and calibration

3.1 Precision

Precision may be quantified as repeatability (the closeness of the agreement between the results of successive measurements of the same measurand carried out under the same conditions of measurement) or reproducibility (where the conditions of measurement may include different operators, locations and techniques). Accuracy is defined as the closeness of the agreement between the result of a measurement and a true value of the measurand (JCGM, 2008, see also http://gaw.empa.ch/glossary.html).

Repeatability of the FTIR analyser is determined as the standard deviation of replicate measurements of a gas sample of constant composition, for example a set of measurements of a constant air sample in the sample cell. Figure 4 illustrates the analyser's repeatability with time series (upper panels) and Allan deviation (lower panels) of consecutive 1-min measurements of CO_2, CH_4, CO, N_2O and $\delta^{13}C$ in CO_2 in dry air. For these measurements the cell was slowly flushed with dried air from a high pressure tank, and spectra collected continuously for more than 2 days (54 h). Pressure in the cell was controlled at 1100 hPa.

Allan variance is commonly used to characterise noise in repeated measurements (Allan, 1966; Werle et al., 1993) and expresses the measurement variance as a function of averaging time. In Fig. 4 the plotted Allan deviation is the square root of the Allan variance. If the variance is dominated by white (Gaussian) noise, as should occur in the ideal case when the precision is detector noise limited, the Allan variance should decrease linearly with averaging time and the log plots of Allan deviation in Fig. 4 should have slope of −0.5, as indicated by the dotted lines. From Fig. 4 it can be seen that in most cases the Allan deviation decreases with $\sqrt{\text{time}}$ for at least 30 min. Repeatabilities (as Allan deviations) for averaging times of 1 and 10 min are summarised in Table 2. These repeatabilities meet GAW compatibility requirements for measurements in the unpolluted troposphere (also listed in Table 2) for all species except $\delta^{13}C$ in CO_2.

3.2 Calibration and accuracy

The least squares fitting of spectra provides concentrations in a raw "FTIR" scale, for which the absolute accuracy depends on the FTIR instrument response, HITRAN line parameters, the MALT spectrum model and the accuracy of the least squares fitting procedure. The raw FTIR measurements are precise as described above, but absolute accuracy is typically less, up to a few percent (Griffith, 2012; Smith et al., 2011). Calibration of the analyser to an absolute or reference scale is achieved by measurements of two or more tanks of air independently calibrated for each trace gas on the reference scales. Griffith et al. (2011) and Hammer et al. (2012) demonstrate that the raw FTIR scale is linear relative to WMO reference scales over a wide range of mole fractions typical of ambient air and above. While the calibration regressions are linear, in general they have small but significant non-zero y-axis intercepts, so the calibration equation for each species is expressed as

$$\chi_{\text{FTIR}} = a \cdot \chi_{\text{ref}} + b \tag{3}$$

where a and b are the coefficients derived from slope and intercept of the regression.

Figure 5 shows residuals from linear regressions of FTIR-measured mole fractions against reference values from a suite of standard tanks maintained at the University of Heidelberg (data from Hammer et al., 2012). Similar measurements over wider mole fraction ranges for a suite of tanks at CSIRO's GASLAB also show no significant deviations from linearity (albeit with lower precision) (Griffith et al., 2011).

3.3 Calibration stability

The Allan variance plots of Fig. 4 (upper panels) illustrate the uncalibrated variability of the FTIR response for continuous 1-min measurements of a single tank gas over a two day period – in general the drift remained within the precision levels summarised in Table 2 over the whole period. Hammer et al. (2012) show similar stability over six days but some species show small significant drifts at the precision limit. Figure 6,

also from Hammer et al. (2012, Fig. 9) illustrates longer-term stability with residuals of approximately daily measurements of a target tank relative to its nominal mole fractions over a 10 month period. The analyser was calibrated against two standards typically every day or two days. The calibration stability for all species except $\delta^{13}C$ in CO_2 meets

5 GAW compatibility standards (Table 1). Hammer et al. (2012) conclude that for most applications weekly calibrations would be sufficient to ensure WMO-GAW compatibility.

3.4 Calibration for $\delta^{13}C$ in CO_2

Griffith et al. (2011) and Loh et al. (2011) have considered isotopologue-specific trace gas calibrations. Spectroscopic analysers such as the FTIR and laser analysers de-

10 termine the mole fractions of isotopologues as individual species, from which the conventional δ values are calculated. In the following, we use IUPAC recommendations (Cohen et al., 2007; Coplen, 2008) to distinguish the following quantities:

C concentration, e.g. $mol\,m^{-3}$

χ mole fraction of trace gas e.g. $\mu mol\,mol^{-1}$, ppm

15 X isotopic abundance of an isotope or isotopologue, $mol\,mol^{-1}$

R isotope ratio

Linestrengths in the HITRAN database (Rothman et al., 2005, 2009) are scaled by the natural abundance for each isotopologue, so that the actual measured isotopologue mole fraction χ_{iso} for an individual isotopologue is reported as the scaled mole fraction

20 χ'_{iso}

$$\chi'_{iso} = \frac{\chi_{iso}}{X_{iso}} \qquad (4)$$

where X_{iso} is the natural isotopologue abundance assumed in HITRAN and shown in Table 3 for the major CO_2 isotopologues (Rothman et al., 2005). With this definition,

FTIR analysis of a sample of CO_2 with all isotopes in natural abundance as specified in HITRAN and perfect calibration would report the same numerical value of χ'_{iso} for each isotopologue.

$\delta^{13}C$ in CO_2 is calculated from the individual mole fractions χ_{636} and χ_{626} and natural abundances X_{636} and X_{626}

$$\delta^{13}C = \frac{\chi'_{636}}{\chi'_{626}} - 1 = \frac{\chi_{636}/\chi_{626}}{X_{636}/X_{626}} - 1 \tag{5}$$

where χ_{636}/χ_{626} is here equivalent to the usual sample isotope ratio R^{13}_{sample} and X_{636}/X_{626} is equivalent to the standard isotope ratio R^{13}_{std}. $\delta^{13}C$ is normally multiplied by 1000 and expressed in ‰, but for clarity the factor 1000 is not explicitly written in the following. The reference scale for $\delta^{13}C$ in Eq. (5) is thus that of HITRAN. Calibration of isotopologue-specific measurements against reference standards calibrated to the standard Vienna Pee Dee Belomnite (VPDB) corrects for both the difference between HITRAN and VPDB scales and calibration factors in the isotopologue-specific FTIR measurements of χ_{636} and χ_{626}, as detailed below.

In applying the calibration Eq. (3) to individual isotopologues, we must know the individual isotopologue mole fractions in the reference standards. For parent and ^{13}C isotopologues of CO_2 these can be calculated from the (assumed known) total CO_2 mole fractions and isotopic δ values for the standard as follows:

The total CO_2 mole fraction is

$$\begin{aligned}\chi_{CO_2} &= \chi_{626} + \chi_{636} + \chi_{628} + \chi_{627} + ... \\ &= \chi'_{626}X_{626} + \chi'_{636}X_{636} + \chi'_{628}X_{628} + ...\end{aligned} \tag{6}$$

From the definition of δ, Eq. (5)

$$\chi'_{636} = (1 + \delta^{13})\chi'_{626}$$
$$\chi'_{628} = (1 + \delta^{18})\chi'_{626}$$
$$\chi'_{627} = (1 + \delta^{17})\chi'_{626} \tag{7}$$

and Eq. (6) can be written

$$\chi_{CO_2} = \chi'_{626} \cdot \left(X_{626} + \sum_i (1 + \delta^i)X_i \right) = \chi'_{626} \cdot X \tag{8}$$

where $X = X_{626} + \sum_i (1 + \delta^i)X_i$ and the index i runs over all isotopologues except 626. Thus

$$\chi'_{626} = \frac{\chi_{CO_2}}{X} \tag{9}$$

and from Eq. (7) the mole fraction of $^{13}CO_2$ is

$$\chi'_{636} = \frac{(1 + \delta^{13}) \cdot \chi_{CO_2}}{X} \tag{10}$$

and similarly for the other isotopologues. To compute X, all values of δ^i and X_i must therefore be known. To calculate individual isotopologue mole fractions via Eq. (10), the total CO_2 mole fraction must also be known. For calibration standards δ^{13} and δ^{18} are usually known, and with sufficient accuracy for FTIR calibrations we can assume $\delta^{17} = 0.5 \cdot \delta^{18}$ and all $\delta = 0$ for multiply-substituted isotopologues since their contributions to the sums are very small.

To generate an isotopologue-specific calibration following Eq. (3) , the reference mole fractions χ_{ref} should be calculated from Eqs. (9) and (10) for the regressions. If calibrated measurements of χ'_{626} and χ'_{636} are used to calculate δ^{13} following Eq. (5), the result should require no further calibration.

However if uncalibrated χ'_{626} and χ'_{636} are used to calculate δ^{13} directly, the result is not simply a linear relation to the reference δ^{13}, because in general it also depends on the mole fraction of CO_2 in the sample as follows from Eq. (5):

$$\delta^{13}_{meas} = \frac{\chi'_{636,meas}}{\chi'_{626,meas}} - 1$$
$$= \frac{a_{636} \cdot \chi'_{636} + b_{636}}{a_{626} \cdot \chi'_{626} + b_{626}} - 1 \tag{11}$$

which can be rearranged to

$$\delta^{13}_{meas} = \frac{a_{636}\chi'_{626}}{a_{626}\chi'_{626} + b_{626}} \delta^{13}_{ref} + \frac{(a_{636} - a_{626})\chi'_{626} + b_{636} - b_{626}}{a_{626}\chi'_{626} + b_{626}}. \tag{12}$$

If the intercepts b are zero, Eq. (12) reduces to a simple scale shift α

$$\delta^{13}_{meas} = \alpha \cdot \delta^{13}_{ref} + (\alpha - 1) \tag{13}$$

where $\alpha = \frac{a_{636}}{a_{626}}$ and the measured and reference δ scales are related by the ratio of isotopologue calibration scale factors a_{636} and a_{626} only. However if b_{636} and b_{626} are non-zero the slope and intercept of Eq. (12) become CO_2 mole fraction dependent and the regression over a range of CO_2 mole fractions is not linear.

There are thus two basic methods to approach $\delta^{13}C$ calibration:

Method 1: absolute calibration

To calibrate δ_{meas} determined by FTIR with reference gases which vary over a range of both δ and χ, δ_{true} can be calculated directly using the true, calibrated values of χ'_{626} and χ'_{636} from Eq. (3). This is demanding on the calibration accuracy, since it requires a full accurate calibration of both isotopologues, and small shifts in the calibration coefficients a and b can lead to significant errors in the δ calibration.

Method 2: empirical calibration

Equation (12) can be rearranged in terms of measured χ'_{626} as

$$\delta_{\mathrm{meas}} = \alpha \cdot \delta_{\mathrm{true}} + (\alpha - 1) + \frac{b_{636} - \alpha \cdot (1 + \delta_{\mathrm{true}}) \cdot b_{626}}{\chi'_{626,\mathrm{meas}}}$$

$$= \alpha \cdot \delta_{\mathrm{true}} + (\alpha - 1) + \frac{\beta}{\chi'_{626,\mathrm{meas}}} \tag{14}$$

where $\beta = b_{636} - \alpha \cdot (1 + \delta_{\mathrm{true}}) \cdot b_{626}$ Eq. (14) reduces to Eq. (13) if the b values are zero.
In Eq. (14) α is a scale shift determined by the isotopologue-specific calibration scale factors $\alpha = a_{636}/a_{626}$, while β quantifies the inverse CO_2 dependence and is determined principally by the difference between b_{636} and b_{626} (since $\alpha \sim 1$ and $\delta \sim 0$).
The inverse CO_2 dependence β can be determined empirically by varying χ at constant δ_{true}. Figure 7a illustrates such a case, where CO_2 is gradually stripped stepwise from a flow of sample air from a tank. The flow is split into two streams in variable portions, one of which is scrubbed completely of CO_2, and the two streams are re-combined. Samples taken from the recombined flow and analysed independently by Isotope Ratio Mass Spectrometry (IRMS) confirmed that there was no fractionation in the stripping process. The inverse dependence on CO_2 mole fraction is observed as expected. Figure 7b shows a regression of $\delta^{13}C$ measured by FTIR and corrected for the empirical CO_2 dependence against reference values for five reference tanks with

CO_2 mole fractions 350–650 µmol mol^{-1} and $\delta^{13}C$ values spanning −8 to −20‰ provided by MPI for Biogeochemistry, Jena. A small non-linearity remains after correction, <0.5‰ across the range of the gases.

3.5 Cross sensitivities

Measured mole fractions of trace gases from the FTIR analyser show small but significant residual sensitivities to pressure, temperature and other trace gases in the sample that are not removed by the spectrum analysis and calibration procedures. These are in general due to imperfections in the measured spectra, systematic errors in the analysis procedure, and systematic errors in temperature and pressure measurements. Hammer et al. (2012) have investigated and quantified these sensitivities in detail for one analyser, and provide a set of linear correction coefficients for sensitivity to cell pressure, cell temperature, flow, residual water vapour and CO_2 mole fractions. These sensitivities are typical of all analysers we have built and tested to date, and are summarised in Table 4. In almost all cases, the sensitivities for reasonable variations in the quantities are small and can be corrected so that uncertainties remain within GAW compatibility targets. These corrections should be applied to raw measured mole fractions before calibration to reference mole fraction scales.

4 Results and selected applications

The FTIR analyser has been used in a variety of applications for atmospheric measurements. An earlier version of the analyser is described by Esler et al. (2000a, b) and some earlier applications are reviewed by Griffith et al. (2000, 2002). Here we review recent applications as examples in clean air monitoring, tower profile measurements and chamber flux measurements which exploit the high precision and stability of the FTIR analyser.

Title Page

Abstract | Introduction

Conclusions | References

Tables | Figures

|◄ | ►|

◄ | ►

Back | Close

Full Screen / Esc

Printer-friendly Version

Interactive Discussion

4.1 Clean air monitoring

A core application of the FTIR analyser is in continuous monitoring of air at background and clean air sites. From November 2008–February 2009 we operated an analyser at the Cape Grim Baseline Air Pollution Station on the NW tip of Tasmania, Australia. Cape Grim samples unpolluted Southern Hemisphere marine air when the airflow is from the SW sector and is a key station of the GAW and AGAGE networks. The detailed results of the 3-month comparison between the FTIR analyser, LoFlo NDIR CO_2 measurements and AGAGE measurements for CH_4, CO and N_2O have been reported previously (Griffith et al., 2011). An overview of the time series is shown in Fig. 8, and details of the comparisons with LoFlo and AGAGE measurements in Fig. 9.

While the LoFlo analyser clearly shows higher precision (less scatter) than the FTIR, for the AGAGE-GC system the FTIR is more precise for each species. Except for CO, for which the AGAGE calibration was uncorrected for detector non-linearity in the GC detector, calibration biases were less than the scatter in the AGAGE data.

4.2 Mobile platforms

The FTIR analyser is portable, robust and automated, and well suited to field applications. We have made FTIR measurements on eight N–S transects of the Australian continent between Adelaide (34° S) and Darwin (12° S) onboard the Ghan train since 2008 (Deutscher et al., 2010). For these measurements the analyser is mounted in a non-airconditioned luggage van and draws air from an inlet on the side of the train. Figure 10 illustrates results for CH_4 during the late wet season of 2008, covering 6 days in which the train travels from Adelaide in the south to Darwin in the north and return. The CH_4 mole fractions show three distinct regions – variable in the agricultural and more populated southern section south of 30° S, low variability and a distinct latitudinal gradient through the arid and unpopulated centre of the continent, and large, irregular enhancements north of 23° S affected by high seasonal monsoonal rainfall. Spikes at 23° S, 14° S and 12° S coincide with long pauses at Alice Springs, Katherine

and Darwin, respectively. The enhanced CH_4 concentrations are attributed mostly to ephemeral emissions from wetlands and are being used to improve methane budgets in the Australian region (Deutscher et al., 2010; Fraser et al., 2011).

Point source emissions detection

The detection, location and quantification of leaks from potential carbon capture and storage sites is of paramount importance for assessing the effectiveness of this technology for removing CO_2 from the atmosphere. In an experiment to assess the possibility of remotely detecting such a leak through atmospheric measurements, Humphries et al. (2012) combined FTIR measurements with a novel tomographic analysis to locate and quantify a point source release of CO_2 and N_2O in a flat, homogeneous landscape. The point source was located within a 50 m circle of 8 sampling points in a bare soil paddock. The sampling points were sequentially sampled and analysed by a common FTIR analyser every 30 min continuously for several months, building up a catalogue of atmospheric concentrations at the 8 sampling points under a range of wind speeds and directions. A Bayesian analysis of the concentration and wind data was used to "find" the location and emission strength for each gas without detailed prior knowledge of either location or emission strength. Figure 11 shows the results of the analysis for the CO_2 release. The analysis located the position of the release within 0.7 m and the strength within 4 %. Similar results were obtained for the N_2O release. The FTIR analyser allowed the continuous autonomous operation of the sampling system for CO_2, N_2O, CH_4 and CO over several months.

4.3 Tower profile and flux measurements

Vertical profiles of trace gas concentrations measured from tall towers and flux towers probe boundary layer mixing processes and trace gas exchange between the atmosphere, surface and plant/forest communities. The Australian Ozflux tower at Tumbarumba (Leuning et al., 2005) is situated in a mature eucalypt forest in SE Australia

to investigate the exchanges of energy, water and carbon in this representative biome. In November 2006 we operated two FTIR analysers at the Ozflux tower over a 3-week campaign, one sampling dried air for precise trace gas measurements, and one sampling undried air for stable water vapour isotope analysis. Seven inlets on a tower from 2 to 70 m above ground were sampled sequentially by both FTIR analysers every 30 min to provide vertical profiles of trace gases, $\delta^{13}C$ in CO_2 and δD in water vapour. The general intent of the campaign was to use vertical profiles of carbon and water isotope fractionations to partition water vapour between evaporation and transpiration, and CO_2 between photosynthetic uptake and release by respiration. The campaign set up and water vapour isotope analysis has been described in detail elsewhere (Haverd et al., 2011). Time series of trace gases and $\delta^{13}C$ are shown in Fig. 12. For CO_2 and $\delta^{13}C$ in CO_2 (Fig. 12a) strong vertical gradients are observed at night when canopy turbulence is low, and there is anti-correlation between CO_2 and $\delta^{13}C$ as the added respired CO_2 is depleted in ^{13}C. Keeling plots such as shown in Fig. 13 show intercepts around −27‰, consistent with respiration from the predominantly C3 plants that dominate this forest. However during daytime, when canopy turbulence is stronger, the air becomes well mixed in the canopy and vertical gradients are smoothed out, making the determination of partitioning from isotopic profiles during daytime impractical. Figure 12b shows similar data for CH_4 and N_2O, indicating clear uptake of CH_4 at the surface (decreasing mole fractions near the ground), and barely detectable N_2O emission (increasing mole fractions near the ground).

Vertical gradients of trace gas concentrations can be used to calculate surface exchange fluxes if the turbulent diffusion can be quantified (e.g. Monteith and Unsworth, 1990). This technique was not practical in the forest environment, where turbulence within the canopy was high during the day and concentration gradients were small, or gradients were high at night but turbulence was suppressed. Flux gradient measurements are suited to agricultural environments above a uniform surface such as grass or crop. Here the high precision of the FTIR analyser is well suited to measurement of the small concentration gradients that exist. An early application to agricultural flux

gradient measurements was able to quantify CO_2 fluxes, but was not sufficiently precise for background N_2O or CH_4 fluxes except following rain when N_2O emissions are enhanced (Griffith et al., 2002). Given the measurement precisions described in Table 2 and a typical turbulent diffusion constant of 0.1–0.2 $m^2 s^{-1}$, Table 5 estimates minimum flux detection limits for the FTIR analyser using the flux gradient technique. Eddy accumulation methods such as Relaxed Eddy Accumulation (REA) or Disjunct Eddy Accumulation (DEA) allow more measurement time to achieve higher trace gas measurement precision, and hence improved flux detection limits. We have applied the FTIR analyser in both REA and DEA techniques, which will be reported in forthcoming publications.

4.4 Chamber measurements

Micrometeorological flux measurement techniques are usually not able to resolve background fluxes of methane, nitrous oxide and trace gases other than CO_2 because the small vertical gradients cannot be resolved with sufficient speed or precicion by existing measurement techniques. In many cases, chamber measurements offer the only feasible method to estimate small fluxes, despite their limitations (e.g. site inhomogeneity and disturbance, microclimate perturbation) (Livingstone and Hutchinson, 1995). The FTIR analyser coupled to automated surface flux chambers provides a useful technique for greenhouse gas exchange measurements at the earth's surface with several advantages:

– Simultaneous measurement of greenhouse gases CO_2, CH_4 and N_2O, as well as CO and $\delta^{13}C$ in CO_2

– High precision enabling the measurement of small fluxes

– High time resolution, with continuous measurements at 1 min resolution or better, allowing assessment of the linearity of concentration changes and hence chamber leakage or other secondary processes occurring in the chamber

– Continuous, fully automated operation

– The isotopic specificity of FTIR analysis allows the option to include isotopic labelling to elucidate the mechanisms of trace gas emissions.

We have carried out several FTIR-chamber flux studies in a variety of agricultural and natural settings. A fully automated system has operated continuously since 2004 measuring N_2O fluxes from irrigated and non-irrigated pasture in Victoria, Australia (Kelly et al., 2008), and another system was applied over a complete sugar cane growth cycle in northern Australia (Denmead et al., 2010). Both studies were based on earlier FTIR systems but provided continuous measurements over periods of months to years.

Here we briefly describe two current examples of chamber flux measurements with the FTIR analyser – full details will be published elsewhere. The Quasom field experiment at the Max Planck Institute for Biogeochemistry in Jena, Germany (https://www.bgc-jena.mpg.de/bgp/index.php/Main/QuasomFieldExperiment) investigates the cycling of carbon through an entire growing cycle of an annual crop by measurements of all carbon pools and fluxes, including isotopic ^{13}C labelling and discrimination measurements. The FTIR analyser is coupled to 12 soil flux chambers in the field experiment and sequentially samples air from the chambers as each goes through a closure cycle. The sampled air is recirculated back to the chambers. The system has operated continuously since June 2011, with a 1-min measurement time and typically ninety 15-min chamber closures per day. The $^{13}CO_2$ isotopic measurements were calibrated using the procedures described in Sect. 3, based on measurements of whole air reference gases provided by MPI-BGC. Results agree well for both absolute and empirical calibration methods, with 1σ precision of better than 0.1‰.

Figure 14 illustrates trace gas measurements from a sequence of closures of seven individual chambers, made in the evening when there is no photosynthetic CO_2 uptake. Individual chambers show considerable variability, but all are sources for CO_2 and N_2O, sinks for CO, and show complex behaviour for CH_4. CO_2 emissions correlate with decreasing $\delta^{13}C$ because the emitted CO_2 is depleted in ^{13}C. Figure 15

shows a typical night-time Keeling plot of $\delta^{13}C$ vs. $1/(CO_2$ mole fraction) from a single chamber closure. The $\delta^{13}C$ signature of the respired CO_2 in the chamber is equal to the y-intercept of the plots, -31.8 ± 0.31‰ and -32.1 ± 0.31‰ for the empirical and absolute calibrations, respectively.

The utility of FTIR analysis for isotopic studies is further illustrated in a recent campaign on an agricultural soil in which ^{15}N labelled substrates (potassium nitrate and urea) were added to soil flux chambers and the emissions of all ^{15}N-labelled N_2O isotopologues ($^{15}N^{14}NO$, $^{14}N^{15}NO$, $^{15}N^{15}NO$) as well as natural $^{14}N^{14}NO$ were determined by the FTIR analyser by analysis of a spectral window near 2200 cm^{-1} in the strong ν_3 band of N_2O (Phillips et al., 2012). The FTIR controlled five soil flux chambers and the FTIR-chamber system ran continuously and automatically for 2 months in December 2011–January 2012 with 1-min time resolution. Chambers were sampled sequentially by the FTIR analyser for 30 min with air recirculated back to the chamber and the chamber closed for 18 min out of each 30 min cycle. Figure 16 illustrates mole fraction measurements for CO_2 and the N_2O isotopologues from one cycle of five chambers after addition of 400 mg N m^{-2} to the soil as $^{15}NO_3^-$ – this represents approximately 10 % of the total soil nitrogen pool. All ^{15}N-N_2O isotopologues could be clearly resolved and quantified with better than 1 nmol mol^{-1} precision. Figure 17 shows the instantaneous and cumulative fluxes of all N_2O isotopologues from 4 days before addition of the ^{15}N label until 8 days after. ^{15}N-labelled N_2O emissions decreased to near-zero levels after 8 days, while emissions of unlabelled N_2O continued from the unlabelled soil nitrogen pool.

5 Conclusions

The FTIR trace gas analyser provides simultaneous, continuous, high precision analysis of the atmospheric trace gases CO_2, CH_4 and N_2O and CO in air. Repeatability meets GAW measurement compatibility standards for clean air measurements, and

Title Page

Abstract | Introduction

Conclusions | References

Tables | Figures

|◀ | ▶|

◀ | ▶

Back | Close

Full Screen / Esc

Printer-friendly Version

Interactive Discussion

with careful calibration accuracy is similar (Hammer et al., 2012). In addition, parallel measurements of $\delta^{13}C$ in CO_2 from the same air samples with precision only slightly less than GAW targets are obtained. The analyser is suited to a wide range of applications in atmospheric trace gas measurements, including composition monitoring at clean air baseline stations and on mobile platforms, micrometeorological and chamber flux measurements, and isotopic measurements in atmospheric trace gases.

References

Allan, D.: Statistics of atomic frequency standards, Proc. IEEE, 54, 221–230, 1966.

Anderson, R. J. and Griffiths, P. R.: Errors in absorbance measurements in infrared Fourier transform spectrometry because of limited instrument resolution, Anal. Chem., 47, 2339–2347, 1975.

Cohen, E. R., Cvitas, T., Frey, J. G., Holmstroem, B., Kuchitsu, K., Marquardt, R., Mills, I., Pavese, F., Quack, M., Stohner, J., Strauss, H. L., Takami, M., and Thor, A. J.: Quantities, Units and Symbols in Physical Chemistry, IUPAC, RSC Publishing, Cambridge, 2007.

Coplen, T. B.: Explanatory glossary of terms used in expression of relative isotope ratios and gas ratios, IUPAC, 27, available at: http://old.iupac.org/reports/provisional/abstract08/coplen_prs.pdf (last access: 16 January 2012), 2008.

Davis, S. P., Abrams, M. C., and Brault, J. W.: Fourier Transform Spectrometry, Academic Press, San Diego, 2001.

Denmead, O. T., Macdonald, B. C. T., Bryant, G., Naylor, T., Wilson, S., Griffith, D. W. T., Wang, W. J., Salter, B., White, I., and Moody, P. W.: Emissions of methane and nitrous oxide from Australian sugarcane soils, Agr. Forest Meteorol., 150, 748–756, doi:10.1016/j.agrformet.2009.06.018, 2010.

5   Deutscher, N. M., Griffith, D. W. T., Paton-Walsh, C., and Borah, R.: Train-borne measurements of tropical methane enhancements from ephemeral wetlands in Australia, J. Geophys. Res., 115, D15304, doi:10.1029/2009JD013151, 2010.

Esler, M. B., Griffith, D. W. T., Wilson, S. R., and Steele, L. P.: Precision trace gas analysis by FT-IR spectroscopy, 1. Simultaneous analysis of CO_2, CH_4, N_2O and CO in air, Anal. Chem.,

10   72, 206–215, 2000a.

Esler, M. B., Griffith, D. W. T., Wilson, S. R., and Steele, L. P.: Precision trace gas analysis by FT-IR spectroscopy, 2. The $^{13}C/^{12}C$ isotope ratio of CO_2, Anal. Chem., 72, 216–221, 2000b.

Francey, R. J., Trudinger, C. M., van der Schoot, M., Krummel, P. B., Steele, L. P., and Langen-felds, R. L.: Differences between trends in atmospheric CO_2 and the reported trends in an-

15   thropogenic CO_2 emissions, Tellus B, 62, 316–328, doi:10.1111/j.1600-0889.2010.00472.x, 2010.

Fraser, A., Miller, C. C., Palmer, P. I., Deutscher, N. M., Jones, N. B., and Griffith, D. W. T.: The Australian methane budget: new insights from surface and train-borne measurements, J. Geophys. Res., 116, D20306, doi:10.1029/2011JD015964, 2011.

20   GAW: Report no. 194, 15th WMO/IAEA Meeting of Experts on Carbon Dioxide, Other Green-house Gases and Related Tracers Measurement Techniques, GenevaWMO/TD-No. 1553, 2011.

Griffith, D. W. T.: Synthetic calibration and quantitative analysis of gas phase infrared spectra, Appl. Spectrosc., 50, 59–70, 1996.

25   Griffith, D. W. T.: FTIR measurements of atmospheric trace gases and their fluxes, in: Handbook of vibrational spectroscopy, edited by: Chalmers, J. M. and Griffiths, P. R., John Wiley & Sons, New York, 2823–2841, 2002.

Griffith, D. W. T.: Non linear least squares retrieval of trace gas concetrations from FTIR spectra, Appl. Spectrosc., in preparation, 2012.

30   Griffith, D. W. T. and Galle, B.: Flux measurements of NH_3, N_2O and CO_2 using dual beam FTIR spectroscopy and the flux-gradient technique, Atmos. Environ., 34, 1087–1098, 2000.

A Fourier transform infrared trace gas analyser

D. W. T. Griffith et al.

Title Page

Abstract | Introduction

Conclusions | References

Tables | Figures

|◄ | ►|

◄ | ►

Back | Close

Full Screen / Esc

Printer-friendly Version

Interactive Discussion

Griffith, D. W. T. and Jamie, I. M.: FTIR spectrometry in atmospheric and trace gas analysis, in: Encyclopedia of Analytical Chemistry, edited by: Meyers, R. A., Wiley, New York, 1979–2007, 2000.

Griffith, D. W. T., Leuning, R., Denmead, O. T., and Jamie, I. M.: Air-land exchanges of CO_2, CH_4 and N_2O measured by FTIR spectroscopy and micrometeorological techniques, Atmos. Environ., 38, 1833–1842, 2002.

Griffith, D., Deutscher, N., Krummel, P., Fraser, P., Steele, P., van der Schoot, M., and Allison, C.: The UoW FTIR trace gas analyser: comparison with LoFlo, AGAGE and tank measurements at CApe Grim and GASLAB, in: Baseline Atmospheric Program (Australia) 2007–2008, edited by: Derek, P. K. A. N., ISBN 978-1-921826-51-1, CSIRO, Melbourne, available at: http://www.bom.gov.au/inside/cgbaps/baseline.shtml (last access: August 2011), 2011.

Griffiths, P. R. and de Haseth, J. A.: Fourier Transform Infrared Spectrometry, 2nd Edn., Wiley, New York, 2007.

Haaland, D. M.: Methods to include Beer's law non-linearities in quantitative spectral analysis, in: Computerised Quantitative Infrared Analysis, ASTM-STP-934, edited by: McClure, G. L., American Society for Testing and Materials, Philadelphia, 78–94, 1987.

Hammer, S., Griffith, D. W. T., Konrad, G., Vardag, S., Caldow, C., and Levin, I.: Assessment of a multi-species in-situ FTIR for precise atmospheric greenhouse gas observations, Atmos. Meas. Tech. Discuss., 5, 3645–3692, doi:10.5194/amtd-5-3645-2012, 2012.

Haverd, V., Cuntz, M., Griffith, D., Keitel, C., Tadros, C., and Twining, J.: Measured deuterium in water vapour concentration does not improve the constraint on the partitioning of evapotranspiration in a tall forest canopy, as estimated using a soil vegetation atmosphere transfer model, Agr. Forest Meteorol., 151, 645–654, 2011.

Hoffman, D. J., Butler, J. H., Dlugokencky, E. J., Elkins, J. W., Masarie, K., Montzka, S. A., and Tans, P.: The role of carbon dioxide in climate forcing from 1979 to 2004: introduction to the annual greenhouse gas index, Tellus B, 58, 614–619, 2006.

Humphries, R., Jenkins, C., Leuning, R., Zegelin, S., Griffith, D., Caldow, C., Berko, H., and Feitz, A.: Atmospheric tomography: a Bayesian inversion technique for determining the rate and location of fugitive emissions, Environ. Sci. Technol., 46, 1739–1746, doi:10.1021/es202807s, 2012.

IPCC: Contribution of Working Group I to the Fourth Assessment Report of the Intergovernmental Panel on Climate Change, Geneva, 2007.

A Fourier transform infrared trace gas analyser

D. W. T. Griffith et al.

Title Page

Abstract | Introduction

Conclusions | References

Tables | Figures

◄ | ►►

◄ | ►

Back | Close

Full Screen / Esc

Printer-friendly Version

Interactive Discussion

JCGM: Evaluation of measurement data – Guide to the expression of uncertainty in measurement (GUM), Joint Committee for Guides in Measurement – Working Group 1, JCGM/WG1JCGM 100:2008, BIPM, September 2008.

Johnson, T. J., Profeta, L. T. M., Sams, R. L., Griffith, D. W. T., and Yokelson, L. R.: An infrared spectral database for detection of gases emitted by biomass burning, Vibr. Spectrosc., 53, 97–102, doi:10.1016/j.vibspec.2010.02.010, 2010.

Keeling, C. D., Whorf, T. P., Wahlen, M., and van der Plicht, J.: Interannual extremes in the rate of rise of atmospheric carbon dioxide since 1980, Nature, 375, 666–670, 1995.

Kelly, K. B., Phillips, F. A., and Baigent, R.: Impact of dicyandiamide application on nitrous oxide emissions from urine patches in Northern Victoria, Australia, Austral. J. Exp. Agric., 48, 156–159, doi:10.1071/EA07251, 2008.

Langenfelds, R., Steele, P., Leist, M., Krummel, P. B., Spencer, D., and Howden, R.: Atmospheric methane, carbon dioxide, hydrogen, carbon monoxide, and nitrous oxide from Cape Grim flask air samples analysed by gas chromatography, in: Baseline Atmospheric Program (Australia) 2007–2008, edited by: Derek, N., and Krummel, P. B., Bureau of Meteorology and CSIRO Marine and Atmospheric Research, Melbourne, ISBN 978-1-921826-51-1, available at: http://www.bom.gov.au/inside/cgbaps/baseline.shtml (last access: August 2011), 62–66, 2011.

Leuning, R., Cleugh, H. A., Zegelin, S. J., and Hughes, D.: Carbon and water fluxes over a temperate *Eucalyptus* forest and tropical wet/dry savanna in Australia: measurements and comparison with MODIS remote sensing estimates, Agr. Forest Meteorol., 129, 151–173, 2005.

Livingstone, G. P. and Hutchinson, G. L.: Enclosure-based measurements of trace gas exchange: applications and sources of error, in: Biogenic Trace Gases: Measuring Emissions from Soil and Water, edited by: Matson, P. A. and Harriss, R. C., Blackwell Science, Cambridge, 1995.

Loh, Z. M., Steele, L. P., Krummel, P. B., van der Schoot, M., Etheridge, D. M., Spencer, D. A., and Francey, R. J.: Linking Isotopologue Specific Measurements of CO_2 to the Existing International Mole Fraction Scale, 15th WMO/IAEA Meeting of Experts on Carbon Dioxide, Other Greenhouse Gases and Related Tracers Measurement Techniques, WMO/GAW report no. 194, Jena, Germany, August 2009, 2011.

Monteith, J. L. and Unsworth, M. H.: Principles of Environmental Physics, Edward Arnold, London, 1990.

A Fourier transform infrared trace gas analyser

D. W. T. Griffith et al.

Title Page

Abstract | Introduction

Conclusions | References

Tables | Figures

Back | Close

Full Screen / Esc

Printer-friendly Version

Interactive Discussion

Parkes, S. D., Element, A., Griffith, D. W. T., Haverd, V., and Wilson, S. R.: An in-situ FTIR analyser for simultaneous real-time water vapour stable isotope and greenhouse gas measurements, Atmos. Meas. Tech., in preparation, 2012.

Phillips, R., Griffith, D. W. T., Dijkstra, F., Lugg, G., Lawrie, R., and Macdonald, B.: Continuous field measurement of N_2O isotopologues using FTIR spectroscopy following ^{15}N addition, in preparation, 2012.

Popa, M. E., Gloor, M., Manning, A. C., Jordan, A., Schultz, U., Haensel, F., Seifert, T., and Heimann, M.: Measurements of greenhouse gases and related tracers at Bialystok tall tower station in Poland, Atmos. Meas. Tech., 3, 407–427, doi:10.5194/amt-3-407-2010, 2010.

Press, W. H., Teukolsky, S. A., Vetterling, W. T., and Flannery, B. P.: Numerical Recipes, Cambridge University Press, Cambridge, 1992.

Prinn, R. G., Weiss, R. F., Fraser, P. J., Simmonds, P. G., Cunnold, D. M., Alyea, F. N., O'Doherty, S., Salameh, P., Miller, B. R., Huang, J., Wang, R. H. J., Hartley, D. E., Harth, C., Steele, L. P., Sturrock, G., Midgley, P. M., and McCulloch, A.: A history of chemically and radiatively important gases in air deduced from ALE/GAGE/AGAGE, J. Geophys. Res., 105, 17751–17792, 2000.

Ravishankara, A. R., Daniel, J. S., and Portmann, R. W.: Nitrous oxide (N_2O): the dominant ozone-depleting substance emitted in the 21st century, Science, 326, 123–125, 2009.

Rothman, L. S., Jacquemart, D., Barbe, A., Benner, D. C., Birk, M., Brown, L. R., Carleer, M. R. C. Chackerian, J., Chance, K., Dana, V., Devi, V. M., Flaud, J.-M., Gamache, R. R., Goldman, A., Hartmann, J.-M., Jucks, K. W., Maki, A. G., Mandin, J.-Y., Massie, S. T., Orphali, J., Perrin, A., Rinsland, C. P., Smith, M. A. H., Tennyson, J., Tolchenov, R. N., Toth, R. A., Auwera, J. V., Varanasi, P., and Wagner, G.: The HITRAN 2004 molecular spectroscopic database, J. Quant. Spectrosc. Ra., 96, 139–204, 2005.

Rothman, L. S., Gordon, I. E., Barbe, A., Benner, D. C., Bernath, P. E., Birk, M., Boudon, V., Brown, L. R., Campargue, A., Champion, J. P., Chance, K., Coudert, L. H., Dana, V., Devi, V. M., Fally, S., Flaud, J. M., Gamache, R. R., Goldman, A., Jacquemart, D., Kleiner, I., Lacome, N., Lafferty, W. J., Mandin, J. Y., Massie, S. T., Mikhailenko, S. N., Miller, C. E., Moazzen-Ahmadi, N., Naumenko, O. V., Nikitin, A. V., Orphal, J., Perevalov, V. I., Perrin, A., Predoi-Cross, A., Rinsland, C. P., Rotger, M., Simeckova, M., Smith, M. A. H., Sung, K., Tashkun, S. A., Tennyson, J., Toth, R. A., Vandaele, A. C., and Vander Auwera, J.: The HITRAN 2008 molecular spectroscopic database, J. Quant. Spectrosc. Radiat. T., 110, 533–572, 2009.

A Fourier transform infrared trace gas analyser

D. W. T. Griffith et al.

Title Page

Abstract | Introduction

Conclusions | References

Tables | Figures

|◄ | ►|

◄ | ►

Back | Close

Full Screen / Esc

Printer-friendly Version

Interactive Discussion

Sharpe, S. W., Johnson, T. J., Sams, R. L., Chu, P. M., Rhoderick, G. C., and Johnson, P. A.: Gas phase databases for quantitative infrared spectroscopy, Appl. Spectrosc., 58, 1452–1461, 2004.

Smith, T. E. L., Wooster, M. J., Tattaris, M., and Griffith, D. W. T.: Absolute accuracy and sensitivity analysis of OP-FTIR retrievals of CO_2, CH_4 and CO over concentrations representative of "clean air" and "polluted plumes", Atmos. Meas. Tech., 4, 97–116, doi:10.5194/amt-4-97-2011, 2011.

Steele, L. P., Krummel, P. D. S., Rickard, C., Baly, S., Langenfelds, R., and van der Schoot, M.: Baseline carbon dioxide monitoring, in: Baseline Atmospheric Program (Australia) 2007–2008, edited by: Derek, N., and Krummel, P., Bureau of Meteorology and CSIRO Marine and Atmospheric Research, Melbourne, ISBN 978-1-921826-51-1, available at: http://www.bom.gov.au/inside/cgbaps/baseline.shtml (last access: August 2011), 51–53, 2011.

Tuzson, B., Henne, S., Brunner, D., Steinbacher, M., Mohn, J., Buchmann, B., and Emmenegger, L.: Continuous isotopic composition measurements of tropospheric CO_2 at Jungfraujoch (3580 m a.s.l.), Switzerland: real-time observation of regional pollution events, Atmos. Chem. Phys., 11, 1685–1696, doi:10.5194/acp-11-1685-2011, 2011.

van der Laan, S., Neubert, R. E. M., and Meier, H. A. J.: A single gas chromatograph for accurate atmospheric mixing ratio measurements of CO_2, CH_4, N_2O, SF_6 and CO, Atmos. Meas. Tech., 2, 549–559, doi:10.5194/amt-2-549-2009, 2009.

Vermeulen, A. T., Hensen, A., Popa, M. E., van den Bulk, W. C. M., and Jongejan, P. A. C.: Greenhouse gas observations from Cabauw Tall Tower (1992–2010), Atmos. Meas. Tech., 4, 617–644, doi:10.5194/amt-4-617-2011, 2011.

Werle, P., Muecke, R., and Slemr, F.: The limits of signal averaging in trace gas monitoring by tunable diode laser absorption spectroscopy (TDLAS), Appl. Phys. B, 57, 131–139, 1993.

A Fourier transform infrared trace gas analyser

D. W. T. Griffith et al.

Title Page

Abstract | Introduction

Conclusions | References

Tables | Figures

◄ | ►

◄ | ►

Back | Close

Full Screen / Esc

Printer-friendly Version

Interactive Discussion

Table 1. GAW measurement compatibility requirements and global mean mole fractions for greenhouse gases.

Species	Approximate global mean mole fraction, 2010 (GAW, 2011)	GAW recommended compatibility target
$CO_2/\mu mol\,mol^{-1}$	389	0.1 (NH) 0.05 (SH)
$CH_4/nmol\,mol^{-1}$	1808	2
$N_2O/nmol\,mol^{-1}$	323	0.1
$CO/nmol\,mol^{-1}$	100 (NH) 50 (SH)	2
$\delta^{13}C\text{-}CO_2/‰$	−8.2	0.01

Table 2. 1σ repeatability (as Allan deviation) for 1 and 10-min averaging times for the FTIR trace gas analyser. GAW compatibility requirements (Table 1) are shown for comparison.

Species	Repeatability (1σ)		GAW compatibility	Unit
	1 min	10 min		
CO_2	0.02	0.01	0.1/0.05	$\mu mol\, mol^{-1}$
CH_4	0.2	0.06	2	$nmol\, mol^{-1}$
CO	0.2	0.08	2	$nmol\, mol^{-1}$
N_2O	0.1	0.03	0.1	$nmol\, mol^{-1}$
$\delta^{13}C$ in CO_2	0.07	0.02	0.01	‰

D. W. T. Griffith et al.

Table 3. HITRAN isotopologue natural abundances.

Isotopologue	Notation	Abundance X_{iso}
$^{12}C^{16}O_2$	626	0.98420
$^{13}C^{16}O_2$	636	0.01106
$^{12}C^{18}O^{16}O$	628	0.0039471
$^{12}C^{17}O^{16}O$	627	0.000734

Table 4. Linear sensitivities $d\chi/d(\text{quantity})$ of trace gas measurements to quantities pressure, temperature, flow and other trace gases in the sample. From Hammer et al. (2012).

$\dfrac{d\chi}{d(\text{quantity})}$	CO_2 $\mu mol\,mol^{-1}$	$\delta^{13}C - CO_2$ ‰	CH_4 $nmol\,mol^{-1}$	CO $nmol\,mol^{-1}$	N_2O $nmol\,mol^{-1}$
Pressure hPa	0.0085	0.005	0.031	0.006	0.007
Equil. Temp. °C	< 0.8	0.6	< 1.6	< 1	0.6
Disequil. Temp. °C	2.07	4.1	−4.6	10.2	3.2
Flow l min^{-1}	0.15	−0.9	< 4	< 2	< −0.8
Residual H$_2$O $\mu mol\,mol^{-1}$	0.04	–	< 0.2	< 0.2	–
CO_2 $\mu mol\,mol^{-1}$	–	0.006[*]	–	0.006[**]	0.008[**]

[*] CO_2 sensitivity is more accurately treated as proportional to inverse mole fraction as described above.
[**] These cross sensitivities reduce to near-zero by using the narrower spectral window shown in Fig. 3b for analysis.

Table 5. Minimum detectable fluxes achievable with the FTIR analyser using the flux gradient technique under typical turbulent diffusion conditions.

	Gradient measurement precision	Minimum detectable flux
CO_2	$0.1\ \mu mol\ mol^{-1}$	$0.04\ mg\ CO_2\ m^{-2}\ s^{-1}$
N_2O	$0.1\ nmol\ mol^{-1}$	$20\ ng\ N\ m^{-2}\ s^{-1}$
CH_4	$0.2\ nmol\ mol^{-1}$	$30\ ng\ CH_4\ m^{-2}\ s^{-1}$
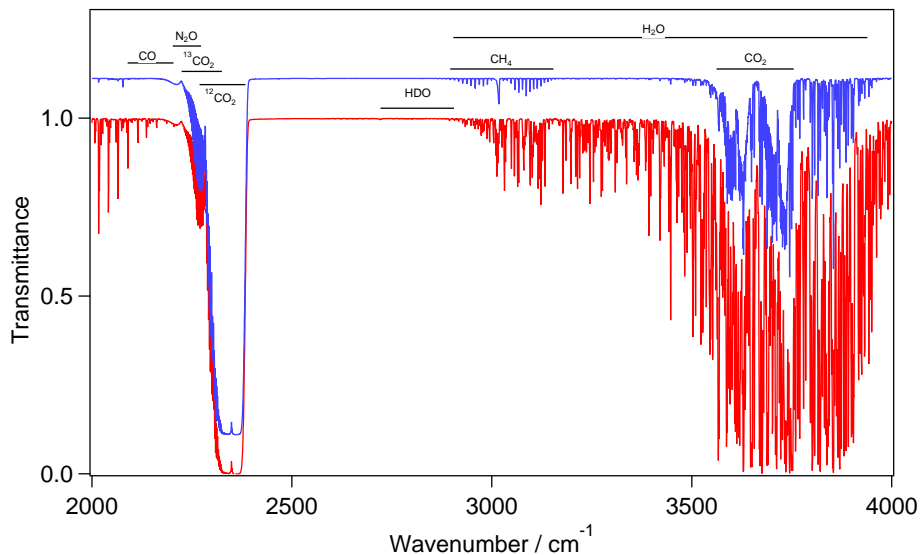
Fig. 1. The mid-infrared spectrum of clean air in a 24 m cell. Red: undried air, blue: dried air. Positions of main absorption bands of target gases CO_2, CH_4, CO and N_2O are shown. More detail of individual regions is shown in Fig. 3.
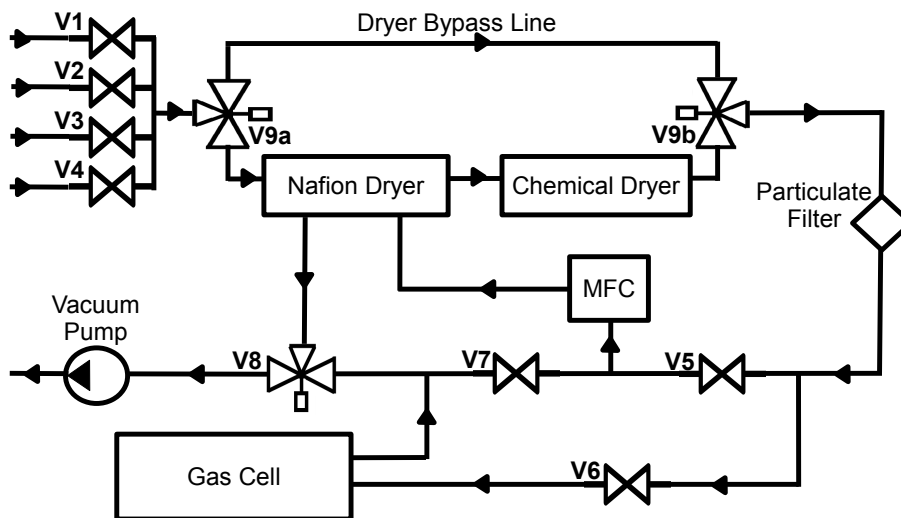
Fig. 2. Schematic view of the sampling gas manifold. For valve functions see text.
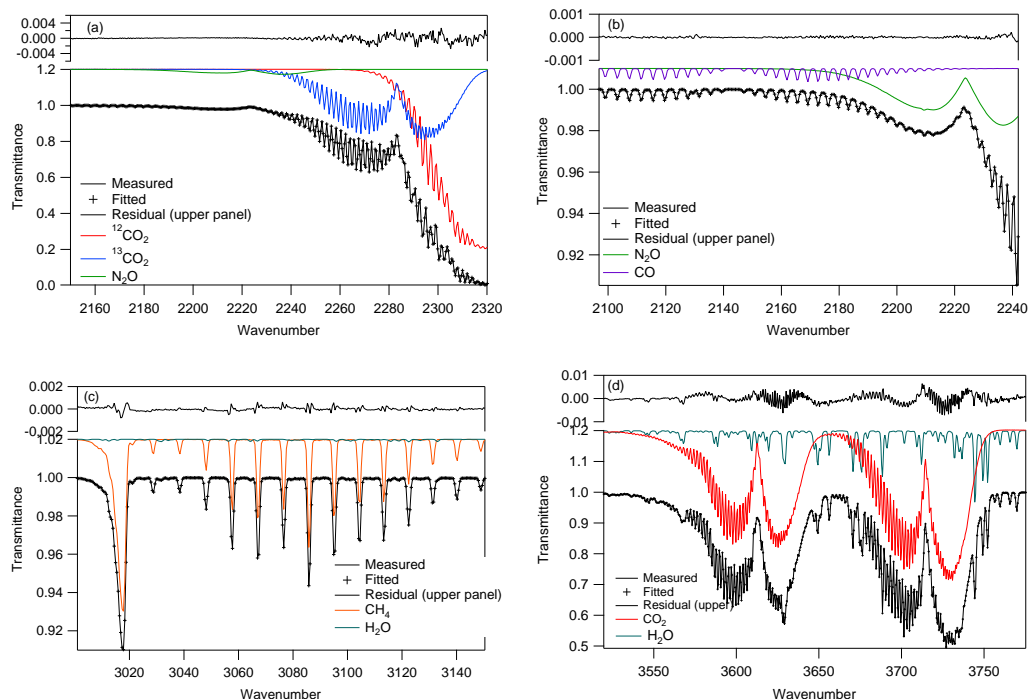
Fig. 3. Typical non-linear least squares fits to a spectrum of dry air in four spectral regions. **(a)** 2150–2310 cm^{-1}, fitting CO_2 isotopologues, CO, N_2O and H_2O; **(b)** 2097–2242 cm^{-1}, optimised for N_2O and CO, also fitting CO_2; **(c)** 3001–3150 cm^{-1}, fitting CH_4 and H_2O; **(d)** 3520–3775 cm^{-1}, fitting CO_2 and H_2O. Contributions from individual species are shown in colours, offset +0.2 units for clarity.
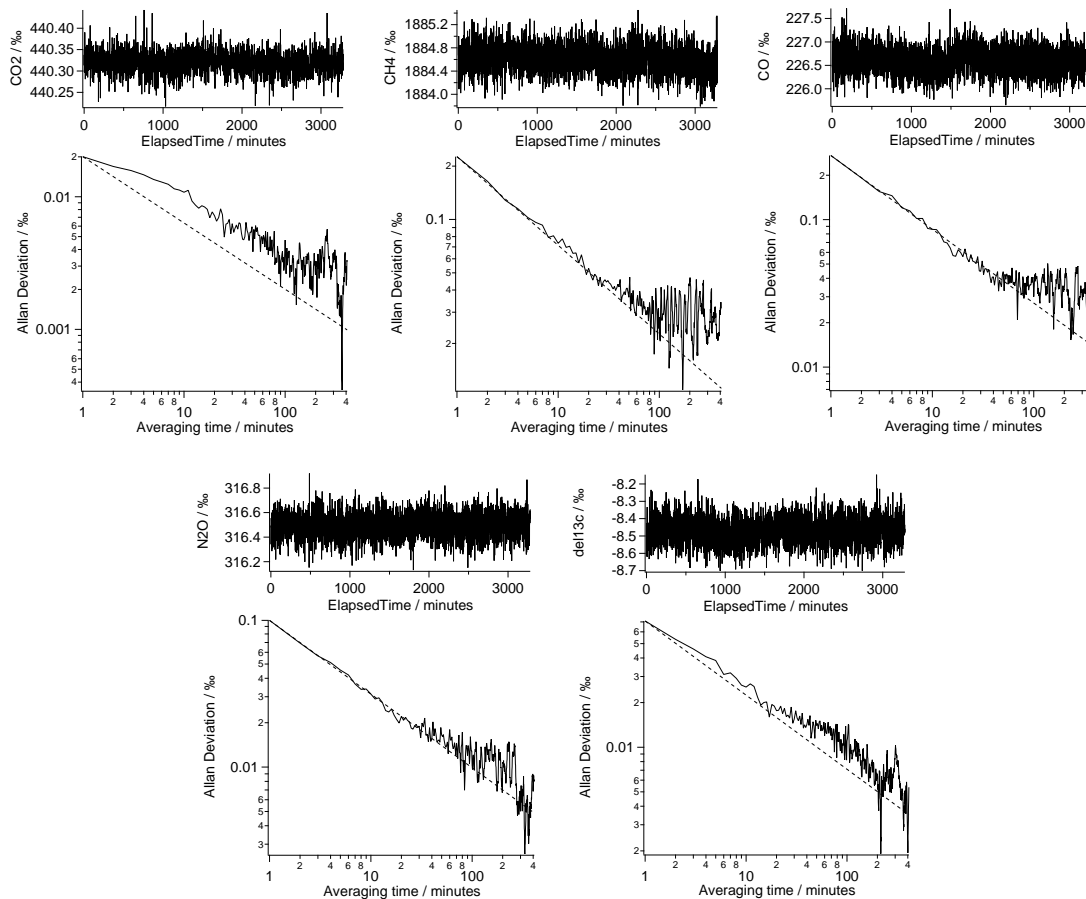
Fig. 4. Time series (upper panels) and Allan deviation (lower panels) plots of consecutive 1-min measurements of CO_2, CH_4, CO, N_2O and $\delta^{13}C$ in CO_2 for an unchanging air sample in the FTIR analyser.

Title Page

Abstract | Introduction

Conclusions | References

Tables | Figures

◄ | ►

◄ | ►

Back | Close

Full Screen / Esc

Printer-friendly Version

Interactive Discussion
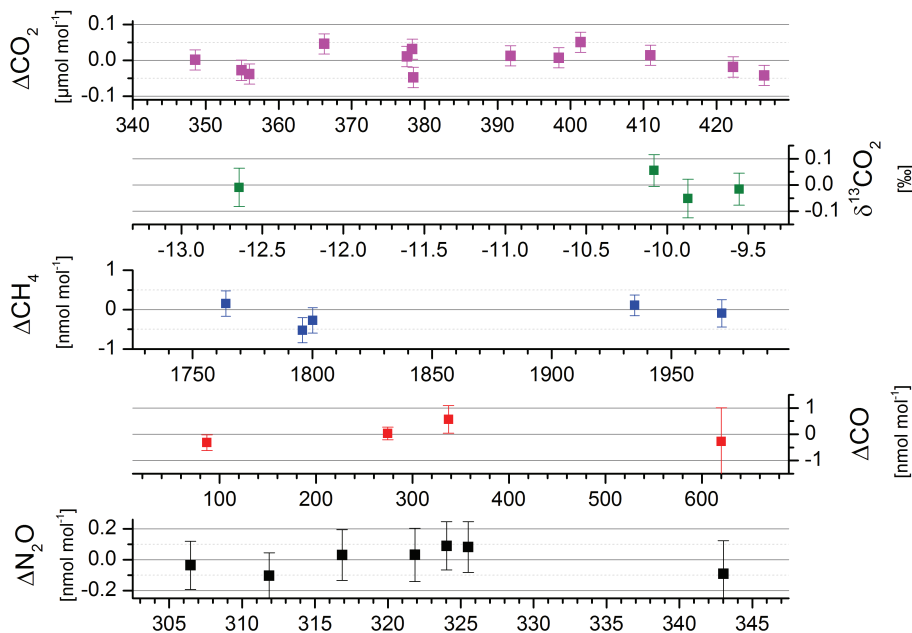
Fig. 5. Residuals from linear regressions of raw FTIR measured mole fractions against reference mole fractions for a suite of tanks maintained by the University of Heidelberg (data and further details from Hammer et al., 2012).
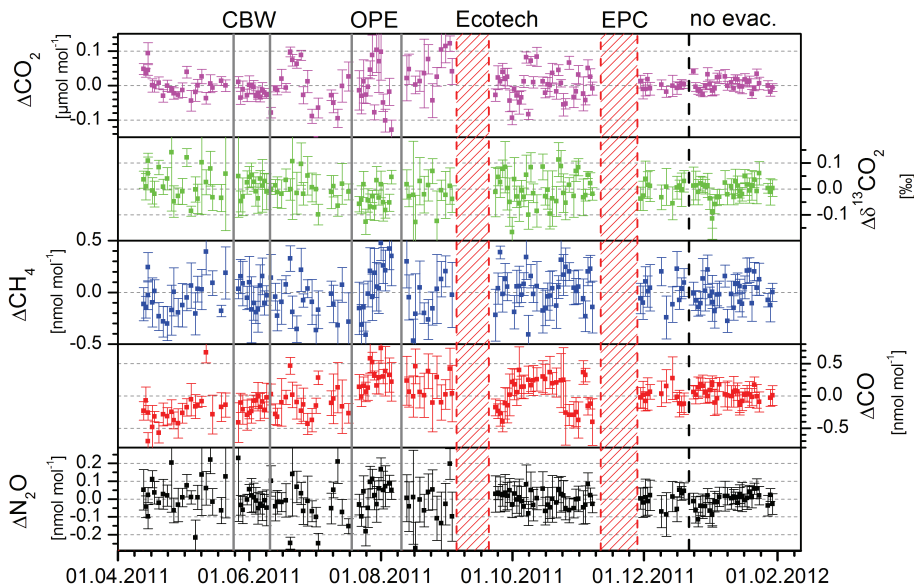
Fig. 6. Measurement residuals relative to a reference value for a single target tank over a 10 month period (Hammer et al., 2012). During this period, the FTIR analyser was based in Heidelberg except for two field campaigns at Cabauw, Netherlands (CBW) and Houdelaincourt, France (OPE). "Ecotech" refers to a rebuild of the instrument to include the mass flow controller (Sect. 2) and "EPC" refers to the addition of an electronic pressure controller upstream of the analyser in the sample airstream. "No evac" refers to a period where ambient and target gas in the cell was exchanged by switching flow alone, without evacuation of the cell.

Title Page

Abstract · Introduction

Conclusions · References

Tables · Figures

|◄ · ►|

◄ · ►

Back · Close

Full Screen / Esc

Printer-friendly Version

Interactive Discussion
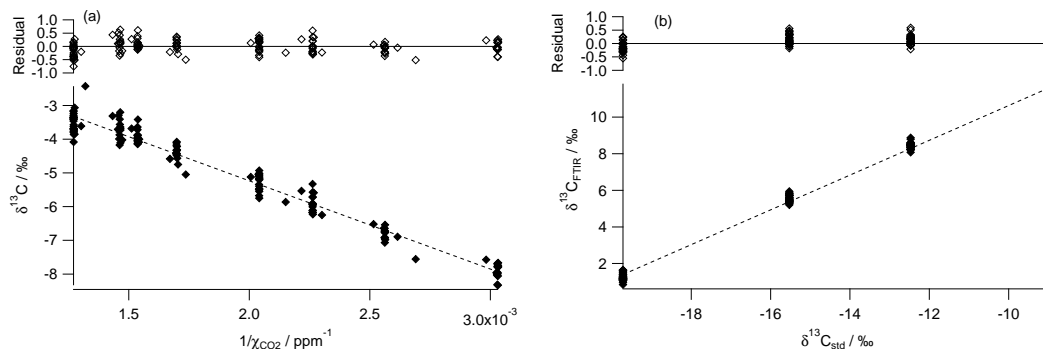
Fig. 7. (a) Empirical dependence of raw measured $\delta^{13}C$ in CO_2 on the inverse CO_2 mole fraction, $1/\chi_{CO_2}$, following Eq. (14). Each point is from a 1 min spectrum measured during the stepwise stripping sequence from 800 to 330 µmol mol^{-1} CO_2. The slope $\beta = -2616$‰ ppm. **(b)** Regression of $\delta^{13}C$ measured by FTIR and corrected for CO_2 dependence using the value of β from **(a)** against reference values for four reference tanks with CO_2 mole fractions 350–650 µmol mol^{-1} and $\delta^{13}C$ values spanning −8 to −20‰. Each point is from a 1-min spectrum after filling the measurements cell with reference gas. A small amount of non-linearity is evident, <0.5‰ across the range.
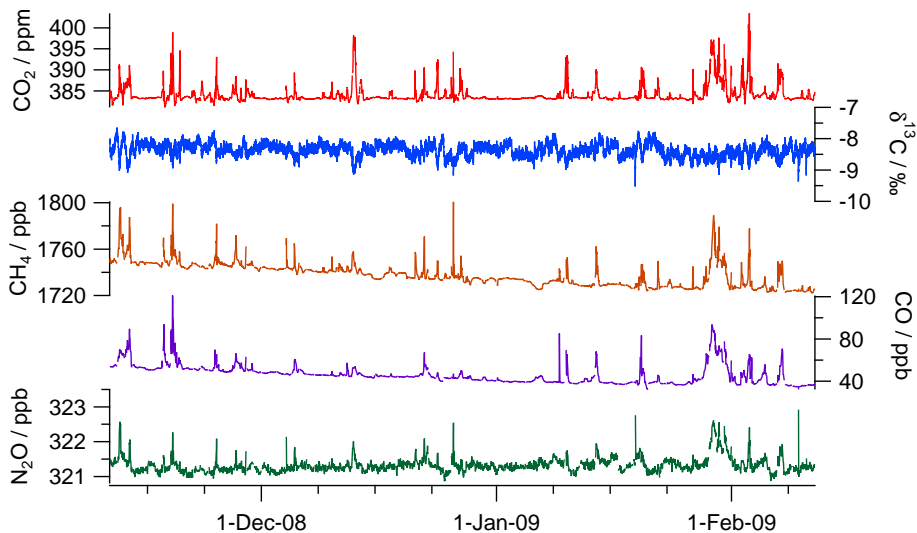
Fig. 8. Time series of trace gas and δ^{13}C measurements at Cape Grim, November 2008–February 2009.
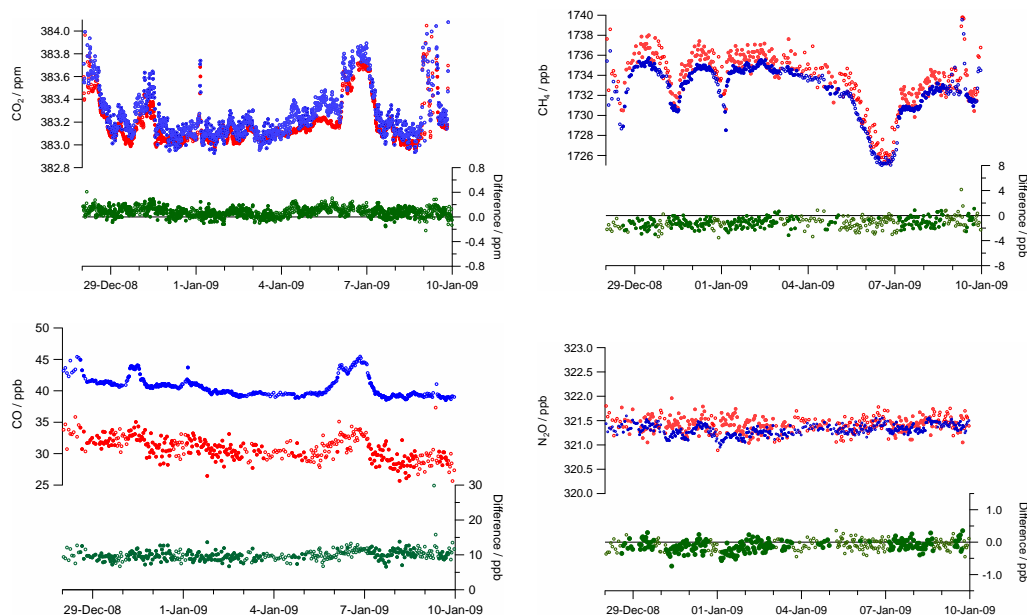
Fig. 9. Detailed comparisons of FTIR measurements with LoFlo (CO_2) and AGAGE (CH_4, CO, N_2O) measurements over a 2-week period at Cape Grim. Red: LoFlo/AGAGE. Blue: FTIR. Upper panels: time-coincident measurements. Lower panels: difference. Full circles represent baseline air periods, open circles non-baseline conditions.
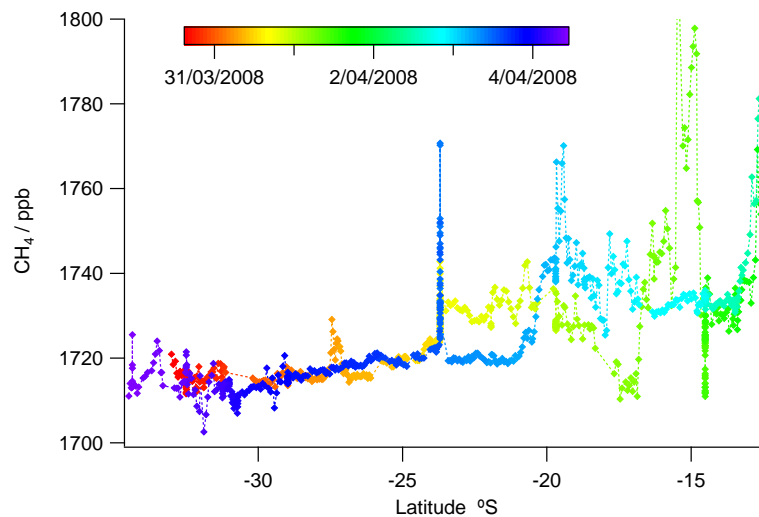
Fig. 10. Measurements of CH_4 along a N–S transect aboard the Ghan train from Adelaide (34° S) to Darwin (12° S), March–April 2008.

Title Page

Abstract | Introduction

Conclusions | References

Tables | Figures

◄ | ►|

◄ | ►

Back | Close

Full Screen / Esc

Printer-friendly Version

Interactive Discussion
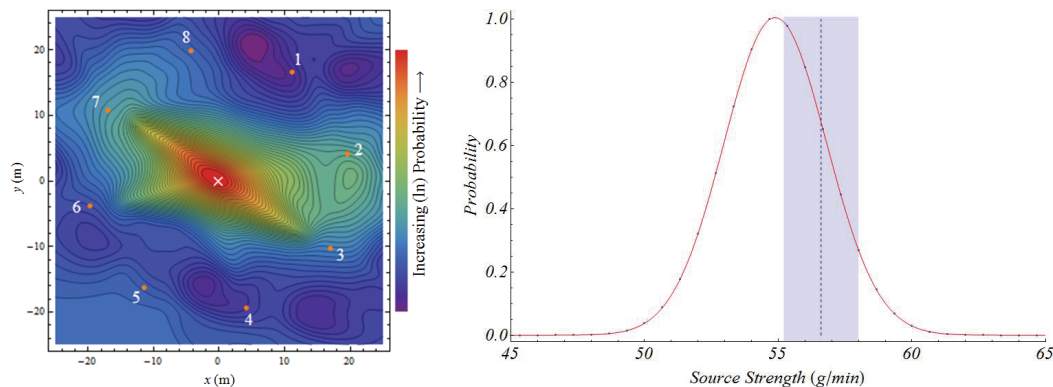
Fig. 11. Result of the FTIR-tomography detection of a CO_2 point source release in a 50×50 m area. In the left hand frame the locations 1–8 of the sampling points are marked, and x marks the actual release point location (0, 0 m). The contours plot the a posteriori probability for the source point location determined from the atmospheric measurements (−0.5, 0.5 m). The right hand plot shows the known release rate (56.7 ± 0.8 g min^{-1}) and the a posterior probability determined from the measurements (54.9 ± 4 (1σ) g min^{-1}). Figure from Humphries et al. (2012), Fig. 5.
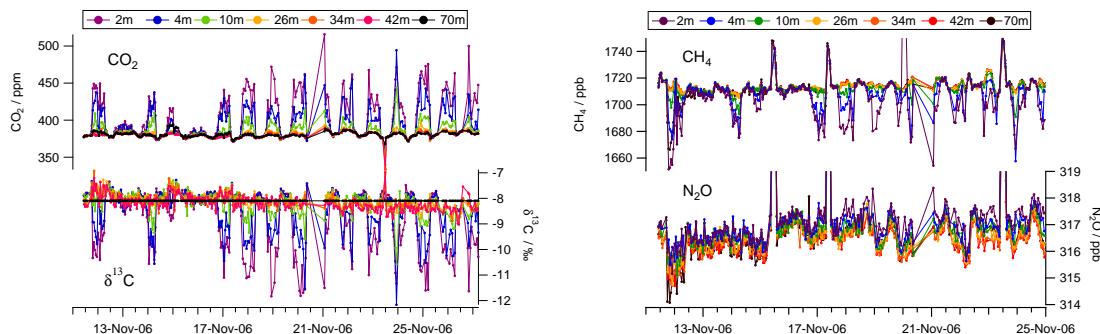
Fig. 12. Time series of trace gas mole fractions and $\delta^{13}C$ in CO_2 for the duration of the Nov 2006 Tumbarumba campaign. Colours represent measurement at different heights above the surface shown in the legend. The top of the forest canopy is approx 40 m above the surface.
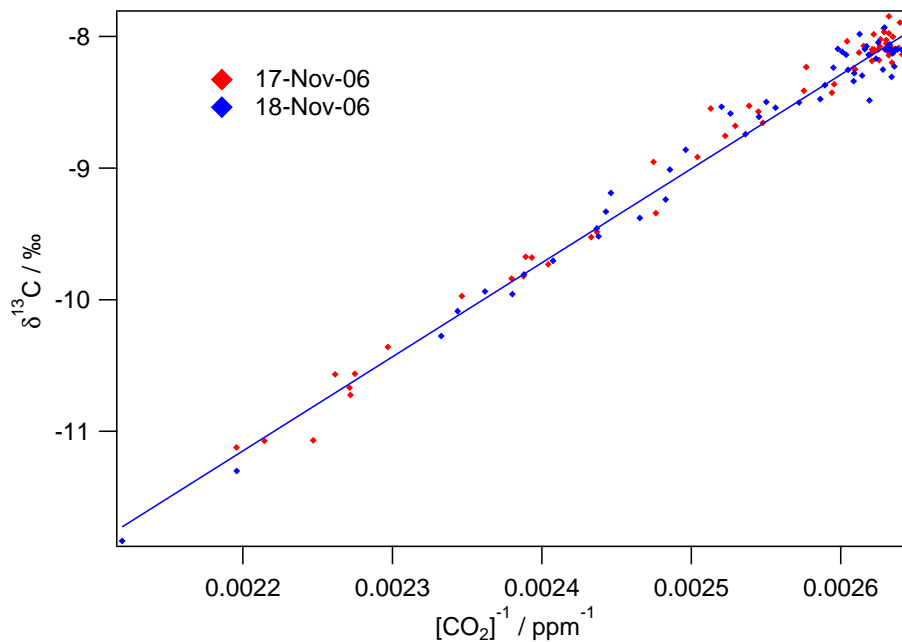
Fig. 13. Keeling plot of δ^{13}C vs $1/[CO_2]$ for two nights on the Ozflux tower. The mean intercept is -26.8‰, indicative of respiration from the dominant C3 plants in the forest.

Full Screen / Esc

Printer-friendly Version

Interactive Discussion
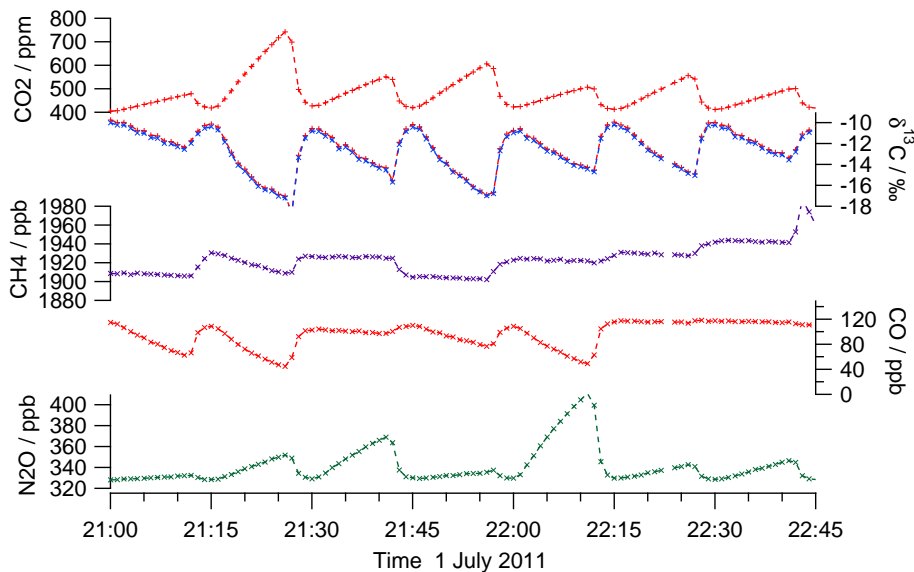
Fig. 14. Time sequence of mole fraction and δ^{13}C in CO_2 measurements from seven sequential chamber closures in the Quasom experiment, 1 July 2011.

A Fourier transform infrared trace gas analyser

D. W. T. Griffith et al.
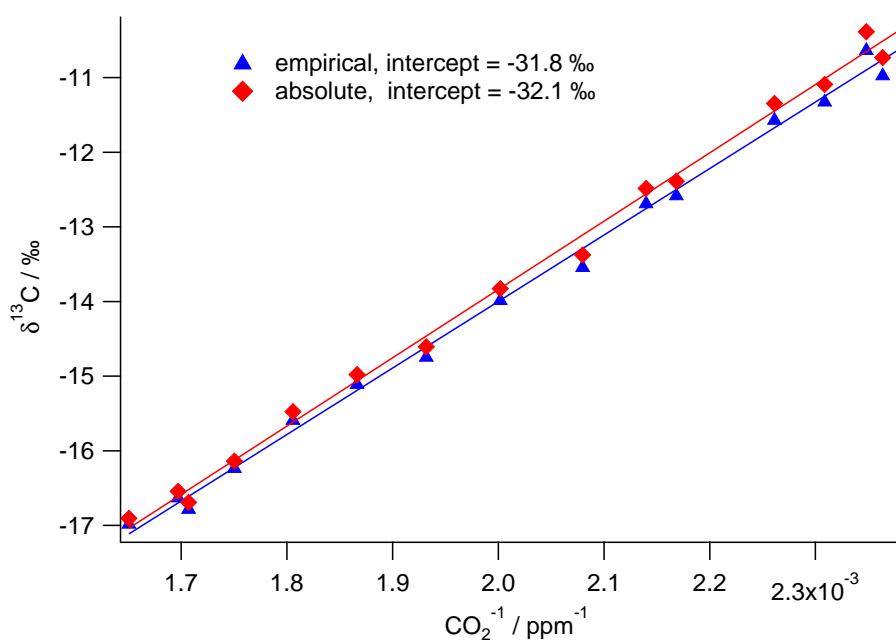
Fig. 15. Keeling plot of δ^{13}C vs. $1/\chi_{CO_2}$ for a typical single chamber closure. The two plots are derived from the absolute and empirical δ^{13}C calibration methods described in Sect. 3.
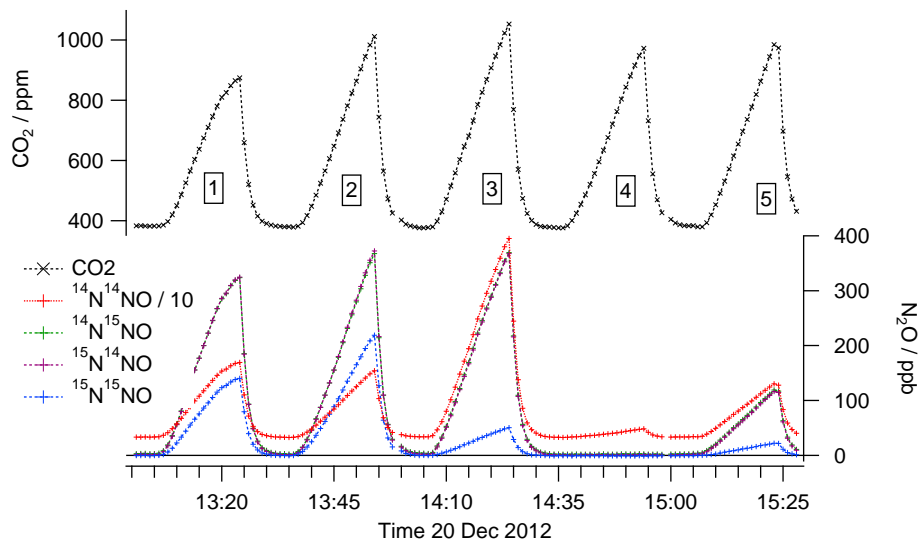
Fig. 16. Time series of CO_2 and N_2O isotopologue measurements in five chambers following addition of ^{15}N as nitrate or urea solution to the soil. Chamber 4 was a blank, where only water without ^{15}N was added.
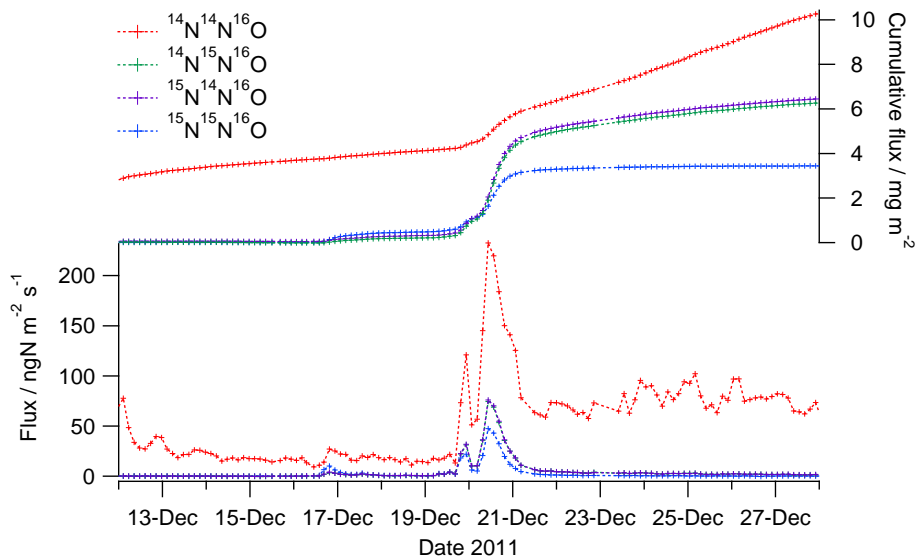
Fig. 17. N_2O isotopologue emissions from one chamber following addition of ^{15}N as nitrate on 17 December. Approximately 25 mm of rainfall fell on 20–21 December 2011.